Universitat de les Illes Balears

BACHELOR'S THESIS

MAGNETOCONDUCTANCE OSCILLATIONS IN TOPOLOGICAL HYBRID JUNCTIONS OF 2D SEMICONDUCTORS

Antonio Alejandro Barreal Rodríguez

Degree in Physics

Faculty of Science

Academic Year 2019-20

MAGNETOCONDUCTANCE OSCILLATIONS IN TOPOLOGICAL HYBRID JUNCTIONS OF 2D SEMICONDUCTORS

Antonio Alejandro Barreal Rodríguez

Bachelor's Thesis

Faculty of Science

University of the Balearic Islands

Academic Year 2019-20

Key words:

Majorana, conductance, nanowire

Thesis Supervisor's Name Llorenç Serra Crespí

Contents

Chapter 1

Introduction

1.1 Motivation

In 1928 Paul Dirac revolutionized the world of physics by interpreting the negative electronic energy solution of his famous equation as the supposed existence of a particle with the same mass but opposite physical charge. This led to the idea that the fermions had a counterpart known as an antiparticle. Years later, in 1937 Ettore Majorana theorized the existence of fermions that were their own antiparticle and the world of science has been searching for this special particle ever since. In particular, it is believed that Majorana states can appear in solids under certain conditions. For example, high conductance plateaus have been found in topological junctions of semiconductor and superconductor material that are signatures of Majorana phases.

Nowadays the goal is to control the appearance of Majorana bound states due to their usefulness in the field of quantum computing. Devices capable of containing Majoranas have the potential to be the basic building blocks of future quantum computers in the same way that the transistor has made today's computers possible.

Our objective in this bachelor thesis is to get an introduction to the world of nanoscience through recent experiments on two dimensional junctions formed by a hybrid side that consists of a superconductor-semiconductor and a normal semiconductor side. Specifically, we want to analyze magnetoconductance oscillations and observe the appearance of topological phases for these systems.

This thesis will begin with background information and theory for the general idea of the physical aspects of normal semiconductor-superconductor systems. Then the model will be presented. As an introduction the Landauer formalism and topological basic concepts will be described.

1.2 Majorana fermions and topological superconductors

As said earlier, Majorana theorized that Dirac's equation could be solved by a particle equal to its antiparticle (identical mass and spin and opposite charge). The Dirac equation reads

$$-i\frac{\hbar}{c}\partial_t\,\psi(\boldsymbol{x},t) = [\,i\hbar\boldsymbol{\alpha}\cdot\boldsymbol{\partial_x} + \beta mc\,]\,\psi(\boldsymbol{x},t), \tag{1.1}$$

where $\boldsymbol{\alpha}$ and β are 4 x 4 matrices, and m is the mass of the particle. The matrices obey:

$$\{\alpha_i,\alpha_j\} = 2\delta_{ij}, \qquad \{\alpha_i,\beta\} = 0, \qquad \beta^2 = 1\ . \tag{1.2}$$

Any $\boldsymbol{\alpha}$ and β satisfying these relations describe a fermion in the relativistic frame. Majorana proposed a basis on which the complex conjugate of Dirac's equation reads

$$-i\frac{\hbar}{c}\partial_t\,\psi^*(\boldsymbol{x},t) = [\,i\hbar\boldsymbol{\alpha}\cdot\boldsymbol{\partial_x} + \beta mc\,]\,\psi^*(\boldsymbol{x},t). \tag{1.3}$$

This means that ψ and ψ^* fulfill the same Dirac equation. The self-conjugated Dirac particle is nowadays called Majorana fermion.

A suitable particle to be a Majorana fermion is the neutrino, but there is still no experimental evidence to confirm this. What about electrons? The electron is a negatively charged particle so it cannot be its own antiparticle directly and therefore is discarded as a Majorana fermion. On the other hand, it has been studied that Majorana fermions can exist as collective excitations of electrons in condensed matter systems.

The collective excitation should satisfy two conditions: obey the Dirac equation and the excitation should be its own antiparticle in the Dirac sense. These special conditions are fulfilled in topological superconductors. First, the boundary excitations obey the Dirac equation because of the topological nature of the superconductor. The second condition is met because superconductors have particle-hole symmetry. This allows Majorana fermions to appear at the edges of topological superconductors.

1.3 Conductance quantization and its relationship with transmission

Van Wees et al. and Wharam et al. [1] carried out independent experiments about the low-temperature conductance of quantum point contacts at zero magnetic field that led to the observation of the conductance quantization. To make it short, the two-dimensional electron gas contributes a gate-voltage independent series resistance in the conductor. Even in a ballistic conductor (that means it has no scattering) the resistance is not zero. If this resistance is subtracted, plateaus appear at quantized values $h/2Ne$ where N is an integer number and e is the electron charge. Due to the resistance discrete values the inverse of the resistance, known as conductance, shows plateau-like values at

$$G = \frac{2e^2}{h} N \ . \tag{1.4}$$

This expression depicts that conductance is quantized in units of twice the conductance quantum $G_0 = \frac{e^2}{h}(\Omega^{-1})$. Experimentally, it is proven that conductance has a limit value reached when the length of the conductor is much shorter than the mean free path of electrons [2]. Then we must consider two effects when describing conductance in low dimensional systems: the length-independent resistance and the fact that conductance takes discrete values. The approach used to describe a conductance with these two features is known as Landauer formalism. Landauer developed a formula for electrical conductance by relating macroscopic properties to quantum mechanics through the probability of transmission

$$G = \frac{2e^2}{h} MT \ , \tag{1.5}$$

where T is the electron transmission probability and M is the number of propagating modes of the conductor. The discrete steps are then related to the transverse modes or subbands in narrow conductors. In this approach we can see that scattering produces

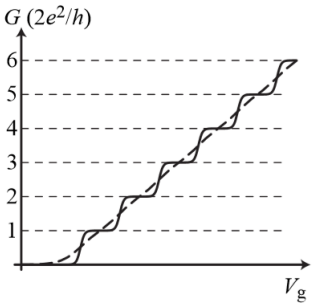

Figure 1.1: Conductance dependence with gate voltage V_g. Image taken from [1].

resistance by reducing the transmission probability. In fact, the total resistance can be separated in two contributions: the interface or contact resistance and a scatterer resistance:

$$R = G^{-1} = G_c^{-1} + G_s^{-1} = \frac{h}{2e^2 M} + \frac{h}{2e^2 M}\frac{1-T}{T} \; . \tag{1.6}$$

The finite quantized conductance without scattering appears due to the power dissipation of the charge carriers in the source and drain contacts.

Chapter 2

Theory and model

This chapter is devoted to the theory and model we use. In the first three sections we introduce, in a general way, the well-known Blonder-Tinkham-Klapwijk (BTK) formalism [3]. This formalism provides as a theoretical starting point to give a preliminary idea of what a normal superconducting junction is. Furthermore, it is the basis used in the calculation of conductance from the transmission probability in the case of an interface modeled as a barrier. Once we had introduced the theoretical starting point, in the remaining sections we discuss the specific model that we use in this work. Our model is based on recent research on the evidence of the existence of Majorana phases in hybrid junctions. In particular, nanowires with two dimensional degrees of freedom in the presence of an applied magnetic field. We discuss the parameters involved and how to find the differential conductance from them. A description of how to find the phases of Majorana modes is also explained.

2.1 The BTK formalism

2.1.1 Generalized semiconductor scheme

A simple semiconductor scheme can be established by taking advantage of the BCS (Bardeen-Cooper-Schrieffer) theory which describes superconductivity from the assumption that it is a microscopic effect caused by the coupling of two electrons (a Cooper pair). In this model the normal state is distinguished from the superconducting by the density of states of the superconductor fase $N_S(E)$ and it is based on the use of the Bogoliubov-de Gennes (BdG) equations [3].

If we only take into account energies $E > \Delta$ (gap energy of the semiconductor), the BdG solutions are for quasiparticle excitations with energy $E_k = \sqrt{\Delta^2 + \epsilon_k^2}$, where $\epsilon_k = \frac{\hbar^2 k^2}{2m} - \epsilon_F$. With each energy there are two possible associated values for k

$$\hbar k^{\pm} = (2m)^{1/2}[\,\epsilon_F \pm (E_k^2 - \Delta^2)^{1/2}\,]^{1/2}. \tag{2.1}$$

In the BCS formalism, the pairing of $-k$ and k generates a fourfold degeneracy of states for each E. This is shown in Fig. 2.1. In this formalism each quasiparticle consists of a linear combination of a hole with momentum $-k$ and an electron with momentum k with opposite spin.

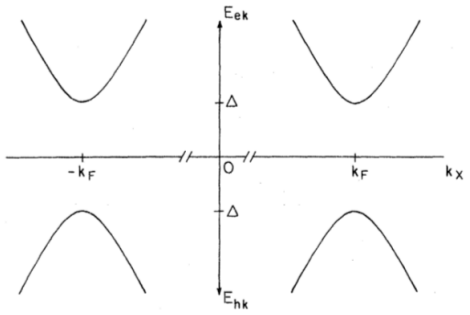

Figure 2.1: Representation of the superconducting excitation energies E_k versus k. Image taken from [3].

To finalize the generalized semiconductor scheme we will focus on the normal metal side. This case is obtained by letting $\Delta \to 0$ in the superconducting approach. In the normal metal this implies that only the branches shown in Fig. 2.2 are possible.

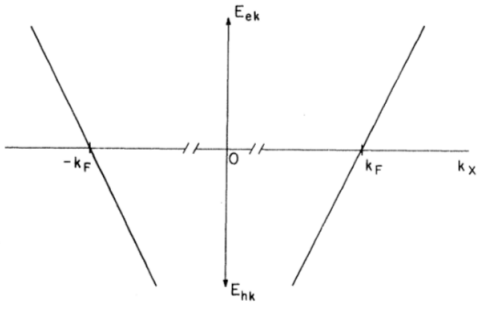

Figure 2.2: Plot of excitation energies for the normal state. Image taken from [3].

2.1.2 Normal-Superconductor interface

In this section, we focus our attention primarily on the N-S interface modeled in the context of reflection with branch crossing, the well-known Andreev reflection. This approach is known as Blonder-Tinkham-Klapwijk (BTK) formalism [3]. The BTK formalism

is a mean-field theory so residual interactions, such as quasiparticle scattering, are not accounted for.

The BTK formalism is based on the BCS theory and the use of the Bogoliubov-de Gennes (BdG) equations. These equations include a series of parameters to characterize superconductors: Hartree potential $V(x)$, pairing strength $\Delta(x)$ and chemical potential $\mu(x)$. By using these equations to handle the interface the problem gets simpler because it can be solved by matching wave functions at the boundary.

In this approach, the superconductor is divided into three different parts: the superconducting regime, the normal regime and the interface between them.

Regarding the interface, the BTK formalism models it as a repulsive delta-function potential $V(x) = H\delta(x)$. We will consider only processes for which energy is conserved and establish that incident particles with positive velocity can generate two processes: transmission of a particle with positive velocity or reflection of a particle with negative velocity. These restrictions simplify the number of allowed processes to four: Andreev reflection if the incident electron coming from the normal side is reflected as a hole; normal reflection if the electron is reflected as an electron; on the other hand, the electron can be transmitted as a hole-like or as an electron-like quasiparticle. The four possible processes are depicted in figure 2.3.

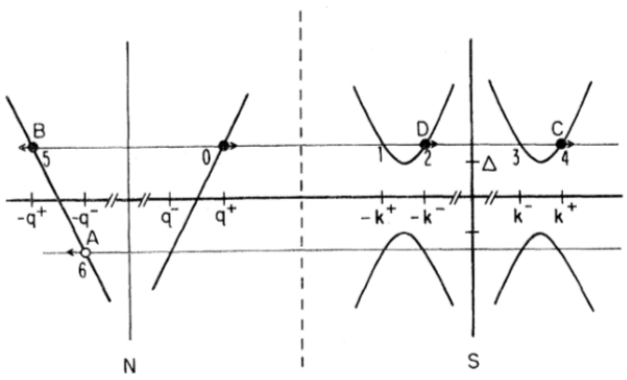

Figure 2.3: Diagram of energy vs. momentum at N-S interface. The empty circles are holes, and full circles electrons. The figure shows the four allowed processes for an incident electron with energy $E > \Delta$ at (0): the Andreev-reflected hole (A), the normal-reflected electron (B), the transmitted electron-like quasiparticle (C) and the transmitted hole-like quasiparticle (D). Image taken from [3].

Considering these four processes the wave functions associated with each possible outcome

for an electron travelling from N to S are:

$$\begin{aligned}
\psi^N_{inc} &= \begin{bmatrix}1\\0\end{bmatrix} e^{ik_+x}, \\
\psi^N_{refl} &= a\begin{bmatrix}0\\1\end{bmatrix} e^{ik_-x} + b\begin{bmatrix}1\\0\end{bmatrix} e^{-ik_+x}, \\
\psi^S_{trans} &= c\begin{bmatrix}u^2_{k0}\\v^2_{k0}\end{bmatrix} e^{ik_+x} + d\begin{bmatrix}v^2_{k0}\\u^2_{k0}\end{bmatrix} e^{-ik_-x} \ .
\end{aligned} \tag{2.2}$$

The prefactors $a-d$ are related to the probabilties of transmission and reflection. In order to obtain them the following boundary conditions are used [4]:

$$\begin{aligned}
&1) \text{ Continuity at } 0: \\
&\psi^N(0) = \psi^S(0) = \psi(0) \ , \\
&2) \text{ Derivative of the wavefunction satisfies}: \\
&\frac{\hbar}{2m}\frac{d\psi^S(0)}{dx} - \frac{\hbar}{2m}\frac{d\psi^N(0)}{dx} = H\psi(0) \ .
\end{aligned} \tag{2.3}$$

Carrying out the algebra one can get the expressions for $a-d$. The probabilities associated with them are: $A(E)$ is Andreev reflection probabilty, $B(E)$ is normal reflection probability, $C(E)$ and $D(E)$ are the transmission probabilites without and with branch crossing, respectively. Their expressions are:

$$\left.\begin{array}{rcl}
A(E) = |a(E)|^2 &=& \frac{u_0^2 v_0^2}{\gamma^2} \\
B(E) = |b(E)|^2 &=& \frac{(u_0^2-v_0^2)^2 Z^2(1+Z^2)}{\gamma^2} \\
C(E) = |c(E)|^2 &=& \frac{u_0^2(u_0^2-v_0^2)(1+Z^2)}{\gamma^2} \\
D(E) = |d(E)|^2 &=& \frac{v_0^2(u_0^2-v_0^2)Z^2}{\gamma^2}
\end{array}\right\} (E>\Delta)$$

$$\left.\begin{array}{rcl}
A(E) &=& \frac{\Delta^2}{E^2+(\Delta^2-E^2)(1+2Z^2)^2} \\
B(E) &=& 1-A \\
C(E) &=& 0 \\
D(E) &=& 0
\end{array}\right\} (E<\Delta), \tag{2.4}$$

where the dimentionless barrier height is defined as $Z = mH/\hbar^2 k_f$ and $\gamma = u_0^2 + (u_0^2 - v_0^2)Z^2$.

2.1.3 Current flowing from N to S. Differential Conductance

When a voltage is applied a current will be generated. In this section, the BTK formalism and the use of BdG equation solutions are still valid [3]. Moreover, we shall assume that equilibrium Fermi functions describe the incoming particles. Following these criteria,

electrons coming from the S side are described by $f_{N\leftarrow S}(E) = f_0(E)$ while those coming in from the N side have $f_{N\rightarrow S}(E) = f_0(E - eV)$. Because of the current conservation the current can be calculated, for simplicity, on the N side. To find this current one must subtract $f_{N\rightarrow S}$ and $f_{N\leftarrow S}$ at two points of the normal side (for example, 0 and 5 on Figure 2.3), and integrate over E:

$$\begin{aligned} I_{NS} &\propto \int_{-\infty}^{\infty} [f_{N\rightarrow S}(E) - f_{N\leftarrow S}(E)]\, dE = ... \\ &= \int_{-\infty}^{\infty} [f_0(E - eV) - f_0(E)]\, [1 + A(E) - B(E)]\, dE. \end{aligned} \tag{2.5}$$

This expression shows that Andreev reflection, $A(E)$, increases the current and normal reflection, $B(E)$ decreases it. From this current expression one can get the differential conductance as follows:

$$\frac{dI_{NS}(V)}{dV} \propto [1 + A(E) - B(E)], \tag{2.6}$$

where the energy is evaluated with respect the apllied bias. This means that $E = eV$.

In Figure 2.4 different plots showing differential conductance at zero temperature versus voltage for different barrier strengths can be seen. In the case of zero barrier strength, $Z = 0$, we see a differential conductance constant value up to the energy Δ which coincides with the energy of the superconducting gap. After this energy value, the differential conductance decays to an asymptotic value. In the rest of the cases, with a barrier strength different from zero, we see that a characteristic peak occurs at Δ. Before this energy the differential conductance takes lower values and for a strong barrier, below energy Δ is practically non-existent. This is a non-trivial result since, despite having a superconducting part, the differential conductance is zero below the superconducting energy gap.

2.2 Model: the 2D-q1D nanowire

Now we are ready to analyse diffential conductance oscillations in topological NS junctions. In our particular case, we are focusing on hybrid nanowires. These are formed when a semiconductor approaches a superconducting material so its superconducting properties are transferred to the semiconductor part. The main feature of these topological systems is that at the ends of the nanowire Majorana modes may appear. To obtain and describe these states, complex band structure is often used. For this purpose, we use recent researches [5] and [6] as a reference for the complex band structure analysis.
In our model we consider a nanowire system, with the axis oriented in the x direction and the transverse directions are characterized by a strong confinement. This is referred as 2D-q1D nanowire which has one transverse degree of freedom, y, and q1D is the acronym

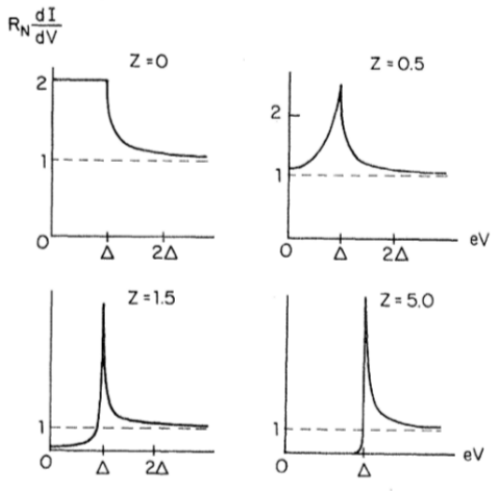

Figure 2.4: This figure shows the BTK model results for differential conductance versus voltage considering different barrier strengths Z at $T = 0$. Image taken from [3].

for quasi-one dimensional system. These type of wires are often called strips.

The model consists of a 2D-q1D nanowire with a normal semiconductor side attached to a hybrid semiconductor-superconductor side. Both sides are separated by a barrier. The continuum coordinates describe the movement in the xy plane and the strip is of width L_y. Isospin and spin are discrete variables described with σ_{xyz} and τ_{xyz} Pauli matrices, separately. Moreover, the magnetic field is perpendicular to the plane, i.e., $B = B_z$, and will affect electron motion in a planar way. The Hamiltonian reads

$$\begin{aligned}\mathcal{H} = &\left(\frac{p_x^2 + p_y^2}{2m} - \mu\right)\tau_z + \frac{\alpha}{\hbar}\left(p_x\sigma_y - p_y\sigma_x\right)\tau_z + \Delta_B\,\sigma_z + \Delta_0\,\tau_x \\ &+ \frac{\hbar^2}{2ml_z^4}y^2\,\tau_z - \frac{\hbar}{ml_z^2}\,yp_x - \frac{\alpha}{l_z^4}y\,\tau_y\ .\end{aligned} \tag{2.7}$$

where Δ_0, Δ_B and α are respectively the pairing, Zeeman and spin-orbit parameters. The Zeeman energy is $\Delta_B = g^*\mu_B B/2$, the gyromagnetic factor is represented by g^*. The chemical potential is μ. The orbital field terms are the last three in Eq. (2.7) and they depend on the magnetic length $l_z^{-2} = eB/\hbar c$.

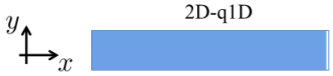

Figure 2.5: Scheme of infinite quasi-one dimensional nanowire along x with y as the transverse dimension. Image taken from [5].

In this approach, the general wave function is represented as

$$\begin{aligned}\Psi(x,y,\eta_\sigma\eta_\tau) &= \sum_{s_\sigma,s_\tau} \Psi^{(k)}_{s_\sigma s_\tau}(y)\, e^{ikx}\, \chi_{s_\sigma}(\eta_\sigma)\, \chi_{s_\tau}(\eta_\tau) \\ &= \sum_k C_k\, \Psi^{(k)}(x,y,\eta_\sigma,\eta_\tau),\end{aligned} \tag{2.8}$$

where $\eta_{\sigma,\tau}$ represent spin and isospin, respectively. For an infinite nanowire and a given wavenumber k, the $\Psi^{(k)}$'s are the eigensolutions. These transverse states of the nanowire give the band structure, $\varepsilon(k)$, from the eigenvalue stationary equation

$$h_k\, \Psi^{(k)}(y,\eta_\sigma,\eta_\tau) = \varepsilon_k\, \Psi^{(k)}(y,\eta_\sigma,\eta_\tau)\ , \tag{2.9}$$

where h_k is the effective 1D Hamiltonian

$$\begin{aligned}h(k) = \left(\frac{(\hbar k)^2 + p_y^2}{2m} - \mu\right)\, \tau_z + \frac{\alpha}{\hbar}\,(\hbar k\sigma_y - p_y\sigma_x)\,\tau_z + \Delta_B\,\sigma_z + \\ \Delta_0\,\tau_x + \frac{\hbar^2}{2ml_z^4}\,y^2\tau_z - \frac{\alpha}{l_z^4}\,y\tau_y\ .\end{aligned} \tag{2.10}$$

In this approach we shall assume that Majorana phase transitions appear as in the 1D case, when the closing and reopening of the gap at $k = 0$ occurs. For this reason, it is only needed the structure given by imposing $k = 0$ on (2.9)

$$h_0\, \Psi^{(0)}(y,\eta_\sigma,\eta_\tau) = \varepsilon_0\, \Psi^{(0)}(y,\eta_\sigma,\eta_\tau). \tag{2.11}$$

2.2.1 Majorana phase boundaries

The general numerical method[1] used in order to obtain phase boundaries of the Majorana is based on wave number analysis with matching conditions on y and spin-isospin components. In the numerical calculation, the equation (2.11) is solved in a 1D grid as a linear system considering fading boundary conditions at the edges. By doing this, the trivial solution can always exist because the system is homogeneous. In order to scrap the trivial solution, a matching point y_m is introduced, and for an arbitrary pair of spin-isospin components a non vanishing wave function is imposed. This method is known as the $\mathcal{F}$-function method and we describe it as in [5].

Equation (2.11) gives the transverse wave functions $\Psi^{(0)}(y, s_\sigma, s_\tau)$ as unknowns. This equation is discretized on a uniform grid for matching point and spin-isospin components $(y, s_\sigma, s_\tau) \neq (y_m, s, t)$. The matching conditions required are

[1] This final degree project does not focus on developing a new numerical model, but on obtaining results from already existing ones. Therefore, only a brief description of the algorithm is given. A more detailed description of the numerical model can be found, for example, in [7].

$$\begin{cases} \Psi_{s,t}(y_m) = 1 \\ \left(\frac{d^{(L)}}{dy} - \frac{d^{(R)}}{dy}\right) \Psi_{s_\sigma,s_\tau}(y_m) = 0 \qquad (s_\sigma, s_\tau) \neq (s,t), \end{cases} \tag{2.12}$$

$d^{(L,R)}/dy$ represent derivatives with only left (L) or right (R) grid neighbours. The first condition makes the system inhomogenous so that it always admits a solution. The second condition is used to discard non-physical solutions with the so called $\mathcal{F}$-function and it reads

$$\mathcal{F} = \left| \left(\frac{d^{(L)}}{dy} - \frac{d^R}{dy}\right) \Psi(y_m, s, t) \right|^2 . \tag{2.13}$$

When $\mathcal{F} = 0$, with fixed k and energy, Majorana phase boundaries appear while sweeping the remaining parameters.

2.2.2 Majorana states

In this section we briefly explain the procedure for calculating the Majorana states[2]. Once the regions with Majorana states have been determined, they can be calculated using complex band theory. To do so, we are interested in obtaining the Majorana wave function previously shown in equation (2.8). In order to do it, a set of complex wave numbers and transverse wave functions $\left\{k, \Psi^{(k)}_{s_\sigma,s_\tau}(y)\right\}$ is calculated first by using sparse non-Hermitian matrix diagonalization techniques. Then, the amplitudes C_k are obtained from the boundary condition at $x = 0$ considering a semi-infinite strip with $x \geq 0$

$$\sum_k C_k \, \Psi^{(k)}_{s_\sigma,s_\tau}(y) \equiv \sum_k \mathcal{M}_{k'k} \, C_k = 0, \tag{2.14}$$

where

$$\mathcal{M}_{k'k} = \sum_{s_\sigma,s_\tau} \int dy \, \Psi^{(k')*}_{s_\sigma,s_\tau}(y) \, \Psi^{(k)}_{s_\sigma,s_\tau}(y). \tag{2.15}$$

The C_k's are then obtained as the diagonalization of $\mathcal{M}$ in equation (2.14). Eventually, the wavefunction is obtained from amplitudes C_k's of the infinite nanowire modes. The Majorana state is built as a linear superposition of these amplitudes.

[2]In this bachelor's thesis it is not necessary to calculate these states but it is described how they are calculated for completeness.

2.2.3 NS hybrid junctions in 2D-q1D

As we mentioned previously we are interested in normal-superconductor junctions and, particularly, junctions of normal lead and hybrid nanowire. The system is formed by a right superconductor contact and a left normal semiconductor contact with an interface central region [6]. The same Hamiltonian describes both regions but the left has a zero superconductor coupling and the right has a finite value. In the central region the coupling can have a position-dependent value.

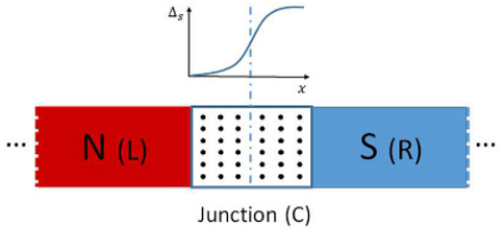

Figure 2.6: Schematic of the NS junction. We distinguish the left (normal), central and right (superconducting) sides. The superconductor coupling Δ_s increases with x position. Image taken from [5].

Solutions with similar form to those of a semi-infinite nanowire are written to describe the ingoing and outgoing propagating modes

$$\Psi(x, y, \eta_\sigma, \eta_\tau) = \sum_{\alpha, n_\alpha} d_{n_\alpha}^{(\alpha,c)}\, e^{ik_{n_\alpha}^{(\alpha,c)} x}\, \phi_{n_\alpha}^{(\alpha,c)}(y, \eta_\sigma, \eta_\tau), \tag{2.16}$$

where the input and output modes are labeled by $\alpha = i, o$ for the contacts $c = L, C, R$. The parameter n_α is the ordering number. The program gives a set of output amplitudes based on the input amplitudes, for a given energy. The use of energy as a parameter is not a restriction since, as explained before, the differential conductance depends on reflection and transmission probabilities at a certain energy. The closed-system of linear equations that need to be resolved reads

$$(\mathcal{H} - E)\Psi(x, y, \eta_\sigma, \eta_\tau) = 0, \qquad (xy) \in C, \tag{2.17}$$

$$\begin{aligned} \Psi(x, y, \eta_\sigma, \eta_\tau) - \sum_{n_o} d_{n_o}^{(o,c)}\, e^{ik_{n_o}^{(o,c)} x}\, \phi_{n_o}^{(\alpha,c)}(y, \eta_\sigma, \eta_\tau) = \\ \sum_{n_i} d_{n_i}^{(i,c)}\, e^{ik_{n_i}^{(i,c)} x}\, \phi_{n_i}^{(i,c)}(y, \eta_\sigma, \eta_\tau), \qquad (xy, c) \in L/R, \end{aligned} \tag{2.18}$$

$$\sum_{\eta_\sigma,\eta_\tau}\int dy\,\phi^{(o,c)*}_{m_o}(y,\eta_\sigma,\eta_\tau)\,\Psi(x_c,\eta_\sigma,\eta_\tau) - \sum_{n_o} d^{(o,c)}_{n_o}\,e^{ik^{(o,c)}_{n_o}x_c}\,\mathcal{M}^{(oc,oc)}_{m_o,n_o} = \sum_{n_i} d^{(i,c)}_{n_i}\,e^{ik^{(i,c)}_{n_i}x}\,\mathcal{M}^{(oc,ic)}_{m_o,n_i}, \qquad c\in L/R, \tag{2.19}$$

where x_c indicates the x coordinate with respect the grid points. The $\mathcal{M}$ matrix is the same from previous section with the new labelling. These set of matching equations are solved for the output coefficients $d^{o,c}_{n_\alpha}$ which are all the information needed to obtain the conductance.

2.2.4 Conductance calculation

All the previous sections and their respective calculations allow finally to obtain the conductance. Knowing the scattering amplitudes, d, the conductance for a given energy E is

$$G(E)\equiv\frac{dI(E)}{dV}=\frac{e^2}{h}\left[\,N(E)-P_{ee}(E)+P_{eh}(E)\,\right], \tag{2.20}$$

where

$$P_{ee}(E)=\sum_{n_o\eta_\sigma}\left|d^{(o,L)}_{n_o}\right|^2\int dy\left|\phi^{o,L}_{n_o}(y,\eta_\sigma,\Uparrow)\right|^2, \tag{2.21}$$

$$P_{eh}(E)=\sum_{n_o\eta_\sigma}\left|d^{(o,L)}_{n_o}\right|^2\int dy\left|\phi^{o,L}_{n_o}(y,\eta_\sigma,\Downarrow)\right|^2, \tag{2.22}$$

are the normal and Andreev reflection probabilites. We use $\eta_\tau=\Uparrow$ to denote the isospin component for electron and $\eta_\tau=\Downarrow$ for hole. The number of incident electron modes is represented as $N(E)$.

In conclusion, to calculate numerically the differential conductance, three steps are needed: first, the solutions for each contact are obtained, as explained in sections 2.2.1 and 2.2.2; then, the system of equations in section 2.2.3 (the scattering problem) is solved and, finally, knowing the amplitudes and the wave functions, the differential conductance is calculated.

Chapter 3

Results

In this chapter we are presenting the results for the normal semiconductor hybrid superconductor (N-hS) junction, where the superconductor side is topological and can host a Majorana mode localized on the end, close to the junction. An applied magnetic field in vertical direction allows to change the topological phases of the superconducting part. We also consider a barrier between N and hS, at the interface as usual. We are mainly interested in the differential conductance which is calculated from Andreev and normal reflection probabilities, as explained earlier. The results also show the transmission that is not necessary to calculate the differential conductance as we have seen previously. It is represented since the codes calculate it. Furthermore, it is an indicative result important for the physics of the problem.

We consider the parameters as in [6]. Specially, the case corresponding to the figure of that reference which shows the conductance for zero energy ($E = 0$) or infinitesimal bias. The figure is showed below as Fig. 3.1 . The N-hS junction has the same structure as in Figure 2.6.

In this same paper [6], the topological phases with Majorana modes are found following the model described in the previous chapter. The phases with Majorana modes were obtained for a series of values of chemical potential and magnetic field considering zero energy. We use as reference these data that describe the trivial and topological phases but we show the junction conductance dependence with energy or applied bias (which is equivalent to $E = \mathrm{e}V$).

We will take four selected magnetic fields, corresponding to different topological phases of Figure 3.1 and show the dependence with E as this is increased. This will allow us to see the evolution of the junction conductance with the bias and with the applied magnetic field and analyse the different transitions between topological and trivial phases. We

choose the following four cases:

1) Trivial (no Majorana): $B = 0.075$ T
2) Topological (with Majorana): $B = 0.5$ T
3) Trivial: $B = 1.12$ T
4) Topological: $B = 1.6$ T

The following results are in effective units (L_u, E_u). The correspondence with physical units is: for length $L_u = 150$ nm, for energy $E_u = 0.1$ meV. Finally, for magnetic field: $\Delta_B/E_u = 4B/\mathrm{T}$. That is B =1 T corresponds to $\Delta_B = 4\ E_u$.

Figure 3.2c shows normal reflection probability R_N, Andreev reflection probability R_A, transmission T and conductance G as a function of the energy for the cases described above. The main result on Figure 3.2 is that the topological phases (panels b and d) are characterized by a conductance that has a peak at zero energy. This is called a zero-bias anomaly and it is due to the peak of the Andreev reflection at zero energy. In panel b the width of the zero-bias anomaly is approximately 7 μV while for panel d, where the magnetic field is greater, the width is 4 μV. Therefore, we can infer that the greater the magnetic field the smaller the width of the anomaly. The zero-bias anomaly is an important result because it indicates the Majorana state presence. Finally, another result we can observe is that in the topological phases (b and d) Andreev reflection dominates over normal reflection.

We are also interested in the case of a very small barrier at the interface. For this purpose, we consider a 0.02 meV barrier in Fig. 3.3. We obtain that for topological phases the results remain the same, these are not affected by the presence of the barrier, except

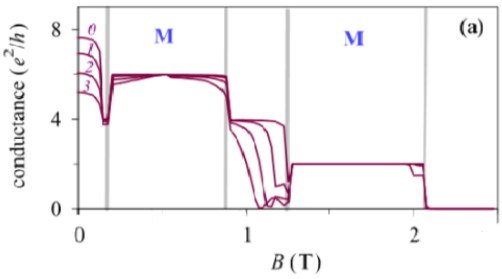

Figure 3.1: This figure shows junction conductance versus the applied magnetic field . The width is L_y=150 nm. The parameters in panel (a) are: spin-orbit coupling $\alpha = 60$ meV nm and chemical potential $\mu = 1.5$ meV. In the graph appear four curves and each one indicates the different barrier strength values at the interface V_0 in meV. The phase transition boundaries are shown by vertical bars. The M indicates the Majorana phase regions. Additional parameters: length of the barrier L_x =7 nm, gyromagnetic factor g^*=15, m =0.033m_e. Image taken from [6].

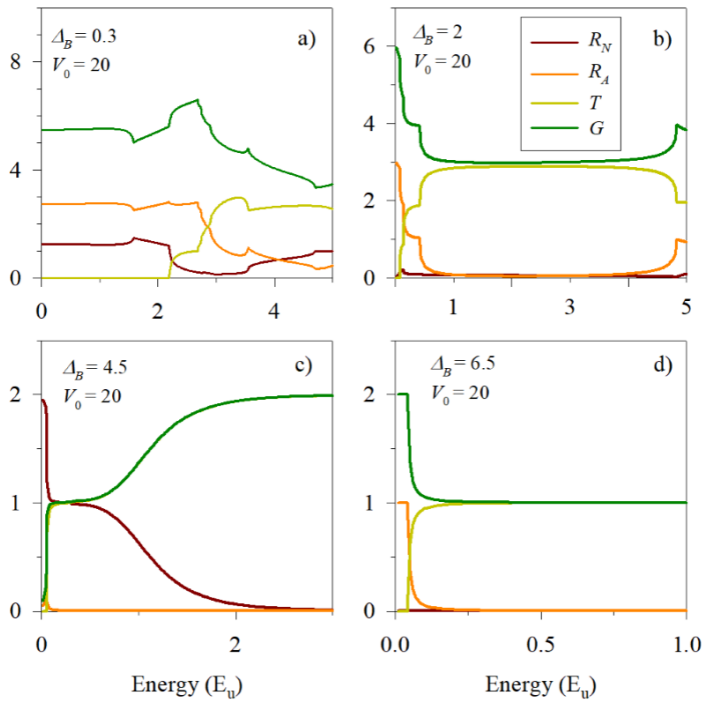

Figure 3.2: Normal reflection probability R_N, Andreev reflection probability R_A, transmission T and conductance G as a function of the energy for the four cases described above. All panels are for SO coupling α =45 meV nm, chemical potential μ =0.5 meV and barrier height V_0 =2 meV=20 E_u. The conductance is in units of the conductance quantum e^2/h. Panel (a) is for magnetic field $\Delta_B = 0.3\ E_u$ (or B=0.075 T); panel (b) is for $\Delta_B = 2\ E_u$ (or B = 0.5 T); panel (c) is for $\Delta_B = 4.5\ E_u$ (or B=1.12 T) and panel (d) is $\Delta_B = 6.5\ E_u$ (or B=1.6 T).

for minor differences. On the other hand, the trivial phases change significantly due to the effect of the barrier. The case c is the one that changes the most. From the BTK model [3] it is expected that the trivial phases without barrier give quantized conductance to infinitesimal bias applied and that is what we are possibly reproducing. In the figure 3.3 the results for a small barrier are shown.

It should be noted that Andreev's reflection is very sensitive to the barrier in the trivial phases. In the topological phases this does not occur and therefore practically the same results are obtained. In panel c, due to the barrier effect the Andreev reflection probability increases so does the conductance. In this case, the width of the zero-bias anomaly present in the topological phases is practically the same; in panel b the width remains 7 μV and in panel d it is 4 μV.

To confirm that we have reached the BTK zero barrier result we also perform the same calculation for an even lower barrier of 2×10^{-4} meV. This is shown in Figure 3.4. The

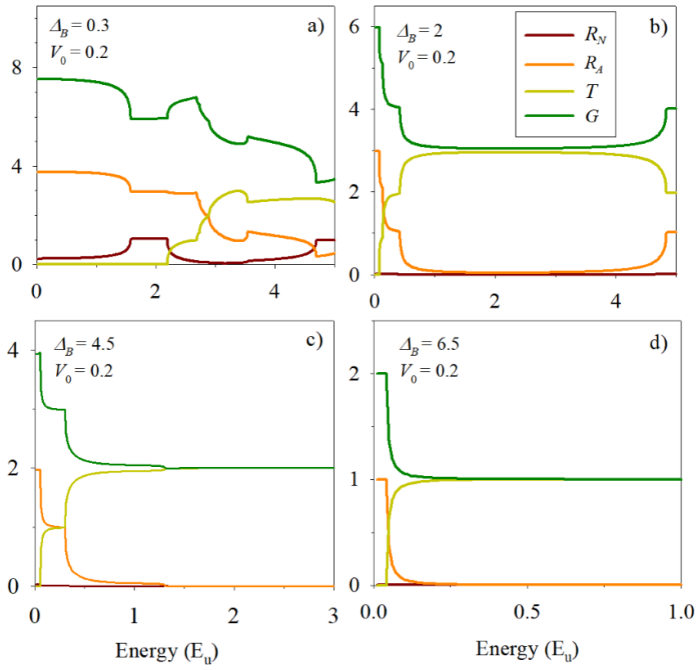

Figure 3.3: Same as Fig. 3.2 for a small barrier $V_0 = 0.02$ meV $= 0.2\ E_u$.

results are identical for both small barriers, confirming that we reached the limit.

We can conclude that the finite bias conductance of the topological NS junction is characterized by a peak near zero (a zero bias anomaly) when the S part is topological and contains a Majorana mode. A barrier at the interface does not change the zero-bias anomaly of topological phases. This has been obtained for the 2D-q1D NS junction in presence of a vertical magnetic field. The magnetic field yields strong orbital effects and allows the S side topological phases of the junction to be controlled. The zero bias anomaly had been discussed previously in 1D wires, but not in planar systems with applied vertical fields as we considered here. In addition, we have seen that the Andreev reflection probability

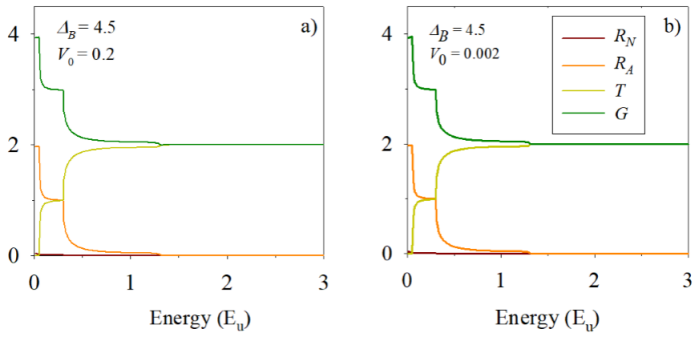

Figure 3.4: Same as Fig. 3.2 for the trivial phase and different barriers. Panel (a) is for barrier V_0 =0.02 meV; panel (b) is for barrier V_0=2×10^{-4} meV.

is very sensitive to changes in the barrier for trivial phases. Finally, regarding the width of the anomaly, we have seen that it does not depend on the barrier but on the applied magnetic field in an inversely proportional way: the greater the applied magnetic field, the smaller the width of the anomaly.

Chapter 4

Conclusions

The realization of this bachelor's thesis has allowed to obtain a first insight into the interesting world of nanoscience, and in particular, a glimpse of transport in nanostructures. We have studied the case of a 2D-q1D nanowire that is relevant to find evidence of the existence of Majorana modes in hybrid normal semiconductor superconductor junctions. In our particular case we have reproduced recent research but focussing on energy dependence. This energy dependence is equivalent to the bias V dependence as $E = eV$.

The novel contribution of this work consists in analyzing the effect of energy that had not been studied for the planar system with a perpendicular magnetic field. In our study we have obtained the well-known zero bias anomaly in differential conductance discussed previously in q1D wires, but not in planar systems with applied vertical fields as we considered here. The results indicate that the width of the zero-bias anomaly depends on the applied magnetic field but does not depend on the barrier strength. In our case, for a 0.5 T magnetic field the width is 7 μV while for a 1.6 T magnetic field the width is 4 μV. When the applied magnetic field increases, the width of the anomaly decreases. Another important result obtained is the relevance of the barrier to distinguish trivial and topological phases. Specifically, in topological phases, changes in the barrier do not affect the differential electrical conductance. On the other hand, in trivial phases the probability of Andreev reflection is sensitive to the strength of the barrier and, therefore, so is the conductance.

As a final conclusion, it should be noted that the work presented here may be expanded in the future. For example, the variation of other parameters such as the chemical potential or the nanowire width could be also studied.

Bibliography

[1] T. Ihn, *Semiconductor Nanostructures: Quantum States and Electronic Transport*. OUP Oxford, 2010.

[2] S. Datta, *Electronic Transport in Mesoscopic Systems*. Cambridge University Press, 1995.

[3] G. E. Blonder, M. Tinkham, and T. M. Klapwijk, "Transition from metallic to tunneling regimes in superconducting microconstrictions: Excess current, charge imbalance, and supercurrent conversion," *Phys. Rev. B*, vol. 25, pp. 4515–4532, 1982.

[4] D. J. Griffiths, *Introduction to Quantum Mechanics (2nd ed.)*. Prentice Hall, 2004.

[5] J. Osca and L. Serra, "Complex band-structure analysis and topological physics of Majorana nanowires," *The European Physical Journal B*, vol. 92, 05 2019.

[6] L. Serra and K. Delfanazari, "Evidence for Majorana phases in the magnetoconductance of topological junctions based on two-dimensional electron gases," *Physical Review B*, vol. 101, 03 2020.

[7] J. Osca and L. Serra, "Majorana modes in smooth normal-superconductor nanowire junctions," *Phys. Rev. B*, vol. 88, p. 144512, Oct 2013.